



The dramatic effect of N-methylimidazole on trans axial ligand binding to ferric heme: experiment and theory

Mohammad Aarabi, Reza Omidyan, Satchin Soorkia, Gilles Grégoire, Michel Broquier, Maria-Elisa Crestoni, Aurélien de La Lande, Benoît Soep, Niloufar Shafizadeh

► To cite this version:

Mohammad Aarabi, Reza Omidyan, Satchin Soorkia, Gilles Grégoire, Michel Broquier, et al.. The dramatic effect of N-methylimidazole on trans axial ligand binding to ferric heme: experiment and theory. *Physical Chemistry Chemical Physics*, 2019, 21 (4), pp.1750 - 1760. 10.1039/c8cp06210b . hal-03007987

HAL Id: hal-03007987

<https://hal.science/hal-03007987>

Submitted on 11 Dec 2020

HAL is a multi-disciplinary open access archive for the deposit and dissemination of scientific research documents, whether they are published or not. The documents may come from teaching and research institutions in France or abroad, or from public or private research centers.

L'archive ouverte pluridisciplinaire **HAL**, est destinée au dépôt et à la diffusion de documents scientifiques de niveau recherche, publiés ou non, émanant des établissements d'enseignement et de recherche français ou étrangers, des laboratoires publics ou privés.

The dramatic effect of N-methylimidazole on trans axial ligand binding to ferric heme: experiment and theory

Mohammad Aarabi^a, Reza Omidyan^a, Satchin Soorkia^b, Gilles Grégoire^b, Michel Broquier^{b,c}, Maria-Elisa Crestoni^d, Aurélien de la Lande^e, Benoît Soep^f, Niloufar Shafizadeh^b.

^a Department of Chemistry, University of Isfahan, 81746-73441 Isfahan, Iran.

^b Institut des Sciences Moléculaires d'Orsay (ISMO), CNRS, Univ. Paris Sud, Université Paris-Saclay, F-91405 Orsay, France

^c Centre Laser de l'Université Paris-Sud (CLUPS/LUMAT), Univ. Paris-Sud, CNRS, IOGS, Université Paris-Saclay, F-91405 Orsay, France

^d Dipartimento di Chimica e Tecnologia del Farmaco, Università degli Studi di Roma "La Sapienza", P.le A. Moro 5, 00185 Roma, Italy

^e Laboratoire de Chimie-Physique, Université Paris Sud, CNRS, UMR 8000. bâtiment 349 Univ. Paris-Sud, Université Paris-Saclay, F-91405 Orsay, France

^f LIDYL, CEA, CNRS, Université Paris-Saclay, UMR 9222 CEA Saclay, F-91191 Gif-sur-Yvette, France.

Abstract

The binding energy of CO, O₂ and NO to isolated ferric heme, [Fe^{III}P]⁺ has been studied in presence or absence of a σ donor (N-methylimidazole or histidine) as *trans* axial ligand. This study joins experimental determination of binding enthalpies by equilibrium measurements in a low temperature ion trap using the van't Hoff equation, and high level DFT calculations. It is found that the presence of N-methylimidazole as axial ligand on [Fe^{III}P]⁺ porphyrin dramatically weakens the [Fe^{III}P-Ligand]⁺ bond with an up to sevenfold decrease in binding energy, owing to σ donation by N-methylimidazole into Fe^{III} (3d) orbitals. This *trans* σ donor effect is characteristic of ligation to iron in hemes in either ferrous or ferric redox forms, yet this has not been observed for ferric heme.

1. Introduction

Hemoproteins are widespread in nature where they operate many functions. One of them is essential, namely oxygen transport. Most hemoproteins utilize at their central core, the Fe atom in its ferrous (Fe^{II}) oxidation state. Nevertheless, ferric (Fe^{III})-heme ($[\text{Fe}^{\text{III}}\text{P}]^+$), is active in many hemoproteins including cytochrome c, and is generally involved in electron transport, while ferrous heme is involved in the transport of small molecules. In turn, ferric heme has a lower affinity for small molecules (O_2 and CO) in *in-vivo* conditions (molecule transport) in difference with ferrous heme. While this affinity is intrinsically small, ferric heme is generally bound to a stronger ligand, H_2O , which is difficult to substitute and thus impedes axial ligation. Nevertheless, protein bound ferric hemes may attach NO or CO in enzymes containing several prosthetic group (hemes), such as the CooA sensor enzyme that is activated by CO^1 .

The coordination number is highly critical for the operation of heme containing proteins, since it crucially determines the affinity to ligands and the redox potentials. Some proteins ligate only in the pentacoordinated state, such as the active site of soluble guanylate cyclase, an enzyme binding NO in 5th coordination to activate its signaling function². There, the coordination of NO is accompanied by the separation from proximal histidine within the protein pocket, this step being essential for the signaling process. The active site is either bound by NO or by histidine, the histidine and NO bonds are not additive and one bond excludes the other. In the following, we shall call 5C (pentacoordinated ligand L) the $[\text{Fe}^{\text{III}}\text{P-L}]^+$ ion with $\text{L}=(\text{NO}, \text{CO}, \text{O}_2)$ and 6C the $[\text{MI-Fe}^{\text{III}}\text{P-L}]^+$ ion with $\text{MI}=\text{N-Methylimidazole}$ and L a second ligand. The Fe atom will be in the oxidized Fe^{III} state, through the paper.

It is therefore important to model the effect of a σ donor ligand in 5th axial position upon the 6C ligation³ in isolated hemes. It may affect the function of blood hemoproteins, where the heme molecule, the Fe protoporphyrin IX adduct (hereafter *all Fe porphyrins* will be labeled $[\text{Fe}^{\text{III}}\text{P}]^+$) is attached to the protein by coordination to an histidine residue. There, the 5th coordinated histidine molecule acts as a σ electron donor to the $3d_{z^2}$ orbital of the Fe atom, which has determining influence on the 6C ligation. We investigate here the importance of a σ electron donor that mimics the coordination of histidine on the affinity of a small molecules O_2 , CO and NO to *ferric heme*. This σ donation effect has also been studied using a small enzyme, microperoxydase MP11, with a bound histidine. The ligand binding energies of $[\text{Fe}^{\text{III}}\text{P-L}]^+$ (5C heme) with $\text{L}=\text{O}_2$, CO and $[\text{MI-Fe}^{\text{III}}\text{P-L}]^+$ (6C heme) with $\text{L}=\text{O}_2$, CO and NO have been deduced from the van't Hoff equation and compared to the calculations performed

at the DFT level. The affinity of O₂, CO and NO to ferric hemes is strikingly diminished in 6C, as measured by the decrease of the binding energy of these ligands and the increase of their calculated Fe-ligand distance. This effect was ascribed earlier to the filling of the 3d_{z²} orbitals by the electrons of the donor^{4,5} (σ donation). Additionally, it has been observed in ref ⁶ and in this work that the attachment of CO as 5th ligand increases notably the affinity for a coordination of another CO in 6th position.

While solution measurements hardly access the observation of 5C hemes because of the blocking ligation to H₂O (or the solvent), only gas phase measurements⁷⁻¹² render the sole or sequential addition of ligands in axial position to heme rather simple, by physically separating the ligation events and avoiding the spurious ligation by H₂O (or the solvent). Following our recent studies on the binding of small ligands to ferric heme¹¹ and protonated heme¹² in a cold, temperature controlled, ion trap, we herein use the same approach with the presence of N-Methyl imidazole (MI) in the iron coordination sphere. The binding energies are deduced through temperature variation in the ion trap, using the van't Hoff equation. These experiments form a basis for comparison with quantum chemistry calculations, which have actively been conducted to characterize the electronic structure of ferric porphyrin and determine bond energies of ligated species.

The spin state of iron porphyrin, as the spin state of any transition metal complex depends on its environment and especially on the nature of its ligand. In the case of ferric porphyrin, three spin states are accessible: doublet (low spin), quartet (intermediate spin) and sextet (and high spin). Figure 1 shows the configurations of Fe atom for S=3/2 and 5/2. The characterization of the spin state of Fe atom is the starting point of the description of the properties of hemes. Indeed, the Fe^{III} atom in the high spin state S=5/2 inflates due to electron repulsion and pops out of the porphyrin cage.

Condensed phase experimental techniques such as Mössbauer spectroscopy or electron spin resonance (ESR) spectroscopy allow ideally the determination of the spin state of iron porphyrins without any ambiguity. Free ferric hemes, are now established in the 3/2 intermediate spin¹³, while ligating with MI induces the high spin (5/2) in [MI-Fe^{III} Octaethyl porphyrin]⁺¹⁴. In turn, gas phase electronic absorption spectroscopy can discriminate low spin state such as NO complexes¹⁵, from intermediate/high spin state¹¹ such as O₂ or N₂

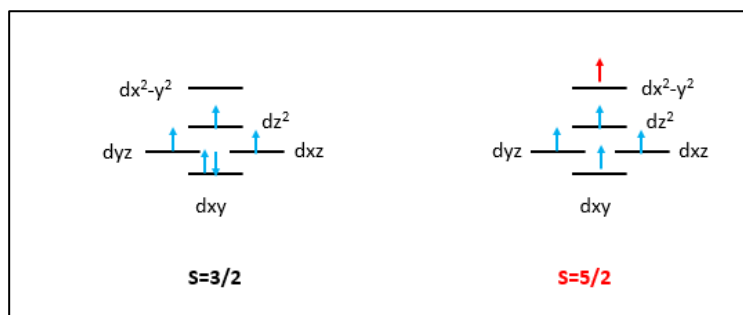


Figure 1: *Fe 3d orbital level structure for the encountered spin states, intermediate spin $S=3/2$ and high spin $S=5/2$. (x, y axes along the Fe-Np bonds.)*

The determination of the electronic configuration of ferric hemes as represented by the spin on the Fe atom is a quite difficult endeavor at the theoretical level. High-level calculations at the DFT level have been conducted to investigate the structure of the 5C and 6C complexes with small ligands and the binding affinity for these ligands. This kind of calculations is non-trivial since the three spin states of the ferric heme are very close, whose positions are utterly sensitive to the functional choice through the exchange and correlation of the five 3d electrons of the Fe atom¹⁶. Calculations on $[\text{Fe}^{\text{III}}\text{P}]^+$ also yield the electronic ground state as a quartet state, as in refs^{9, 17-19}. While calculations were apparently the only method to compare 5C to 6C coordination of ferric hemes in the gas phase^{16, 20-22}, a direct comparison is made here between gas phase results and calculations.

2. Experimental Setup

The experimental setup has been described in details previously^{11, 23}. The setup is composed of three parts: an electrospray ionization source (ESI), a quadrupole ion trap 3D-QIT (Jordan ToF Inc.), and a linear time-of-flight mass spectrometer (TOF). Hemin (Sigma-Aldrich) or MP11 are dissolved in methanol, at a concentration of ~ 100 - $10 \mu\text{M}$. In the case of MP11, a drop of acetic acid has been added to the solution. Ions are produced in the ESI source, stored in an octopole trap for 100 ms and then extracted/accelerated by applying a negative voltage pulse at the octopole exit electrode. This time sequence produces ion packets. The ions are driven by a couple of electrostatic lenses toward the 3D-QIT, biased at ~ 200 V, which matches the energy of the incoming ions. A mass gate placed before the entrance of the 3D-QIT allows the selection of the parent ion. The 3D-QIT is cooled by a compressed helium cryostat (CH-204S, Sumitomo). The temperature of the trap can be precisely monitored over the 10-300 K

temperature range by a cartridge heater and a couple of temperature sensors interfaced to a temperature controller (Lake Shore model 335).

The ions are trapped and thermalized through collisions with the helium buffer gas mixture with 1% ligand, injected by a pulsed valve 1-2 ms before the ions enter the trap. The photodissociation laser for excitation spectra is triggered after a variable storage delay, in the 40-80 ms time range. Ions are then extracted to the mass spectrometer and detected on a microchannel plate detector (Z-Gap MCP, Jordan ToF Inc.). The one-color spectra of $[\text{MI-Fe}^{\text{III}}\text{P-O}_2]^+$ ions are obtained by scanning the laser frequency and recording the signal of the fragments: either $[\text{MI-Fe}^{\text{III}}\text{P}]^+$ for O_2 detachment, or $[\text{Fe}^{\text{III}}\text{P}]^+$ ions for MI and O_2 detachment. The time delay between the photodissociation laser and the extraction is $\sim 40\text{ms}$, leaving the possibility of ground state statistical dissociation. Great care has been taken to monitor single photon absorption by having a large laser interaction surface with ions 3 mm in diameter and matching the laser crosssection with that of the ions in the trap.

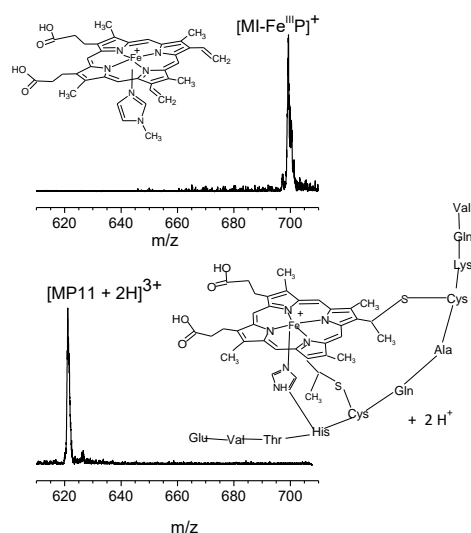


Figure 2: Top, mass spectra of pentacoordinated hemes: pentacoordinated $[\text{MI-Fe}^{\text{III}}\text{P}]^+$ $m/z=698.6$ amu; bottom the triply charged, doubly protonated small protein, microperoxidase11: $[\text{MP11} + 2\text{H}]^{3+}$ $m/z=621.3$ amu

A 10 μM molar methanol solution of hemin $[\text{Fe}^{\text{III}}\text{P-Cl}]$ is coordinated by the addition of a few drops of MI, which binds strongly at room temperature. When submitted to electrospray, this solution delivers $[\text{MI-Fe}^{\text{III}}\text{P}]^+$, which is then injected in the quadrupole ion trap after mass gating the pentacoordinated complex (Figure 1, upper trace). We have also prepared in slightly acidic conditions $[\text{MP11} + 2\text{H}]^{3+}$ (Figure 2, lower panel) from microperoxidase11 (MP11), an

artificial enzyme derived from cytochrome c, by a careful adjustment of the acceleration voltage in the collision zone of the ESI.¹⁰ Then, $[\text{MP11 2H}]^{3+}$ ions are mass-selected and injected in the ion trap. Ligated ferric ions are thus formed in equilibrium conditions in the ion trap with their ligands (NO , CO , O_2) as previously described¹². Equilibrium is easily verified by the complete disappearance of the parent $[\text{Fe}^{\text{III}}\text{P}]^+$ and the linear dependence of the signal of the $[\text{Fe}^{\text{III}}\text{P-L}]^+ / [\text{Fe}^{\text{III}}\text{P}]^+$ ratio with the pressure of the gaseous ligand L at a given temperature. The variation of this ratio with different pressures appears as van't Hoff parallel plots representing $\text{Ln}([\text{Fe}^{\text{III}}\text{P-L}]^+ / [\text{Fe}^{\text{III}}\text{P}]^+)$ and shifted by $\text{Ln}(\text{ligand partial pressure})$.

3. Computational details:

3. 1. *Ferric-Porphyrin heme-Model system*

The molecular model considered in this study is a Fe^{III} -porphyrin cation ($[\text{Fe}^{\text{III}}\text{P}]^+$) with the ligands placed along the perpendicular axis to the plane of the porphyrin ring in 6th axial position with/without MI in 5th axial position as shown in Figure 3. The substituents of heme are replaced by the appropriate number of hydrogen atoms in order to reduce the size of the model, thus the computational cost. It was shown^{20, 24-27} that the chemical and physical properties of heme can be reproduced by this truncated model system. We also replaced the histidine residue by 5-methylimidazole in 5th axial position for its structural similarity with histidine. However, experimentally, the use of N-methylimidazole has been preferred, since there is a tautomeric equilibrium between 4- and 5-methylimidazole. The affinity for the ferric ion of the sp² lone pair orbitals of the N atom in all three systems is nevertheless very similar. We investigated the binding of neutral forms of some biologically important ligands comprising O_2 ($S = 1$), CO ($S = 0$) and NO ($S = 1/2$) to the iron centre of ferric porphyrin. The starting conformational orientation for each ligand was considered as linear, perpendicular to the porphyrin plane, except in the case of O_2 for which a bent structure was assigned, as illustrated in Figure 3. For each complex, we have considered three possible spin states: low-spin ($S = 1/2$, doublet), intermediate-spin ($S = 3/2$, quartet), and high-spin ($S = 5/2$, sextet) except for NO complexes for which the three possible spin states $S = 0$, 1 and 2 (singlet, triplet and quintet, respectively) were considered.

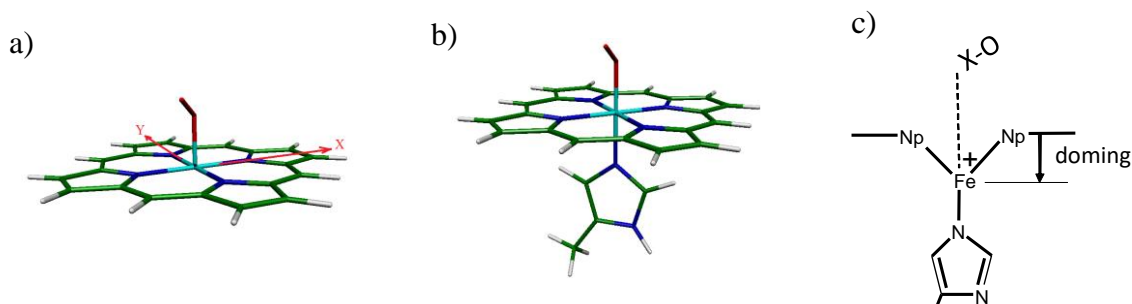


Figure 3: The ferric porphyrin model system for a) $[Fe^{III}P-O_2]^+$, b) $[MI-Fe^{III}P-O_2]^+$ and c) nomenclature and geometry parameters.

3. 2. A-DFT and Full-DFT Calculations

In the present study, all geometry optimizations were performed with deMon2k²⁸ in the framework of auxiliary DFT (ADFT). In ADFT, variationally fitted auxiliary electron densities are used to determine the classical Coulomb repulsion among electrons and the exchange–correlation (XC) contributions. The ADFT leads to considerable savings in computational time. We used the OPTX exchange functional proposed by Cohen and Handy, coupled to the Perdew–Becke–Ernzerhof (PBE) correlation functional. A double- ζ valence polarization basis set calibrated for Generalized Gradient Approximation (GGA) functionals has been used (DZVP-GGA). All calculations have been performed within the unrestricted Kohn–Sham (UKS) formalism. Auxiliary electron densities were expanded with automatically generated GEN-A2 auxiliary basis set on C, H and the larger GEN-A2* basis set (including f and g orbital angular momentum functions) on the Fe, O and N atoms of ligands. It should be emphasized that typically optimized ADFT geometries are indistinguishable from DFT calculations without density fitting (DF), even for weakly bound systems. Differences between ADFT and DFT geometries are usually in the range of the accuracy of the underlying approximate exchange–correlation functional²⁹. Therefore the choice of the more flexible Gen-A2* auxiliary basis set for Fe, O and N atoms permits an accurate description of metal–ligand bonding.

No symmetry constraints were applied during geometry optimizations. To integrate the XC energy and potential, an adaptive grid of high accuracy has been used (10^{-8} Ha). Additionally, dispersion effect corrections were also considered by an empirical expression in all calculations

since it has been demonstrated that including dispersion interactions improves the calculated binding energies for transition metal complexes^{30, 31}, especially iron porphyrin ones^{20, 27}.

In heme-related complexes, the calculation of the stability of different spin-states in their ground electronic state and the binding energies of different ligands to $[\text{Fe}^{\text{III}}\text{P}]^+$ systems are challenging issues. In the last two decades, a vast numbers of experimental and theoretical reports have been devoted to this topic^{6, 11, 16, 26, 32-43}. However, the main problem arises in transition metals with a half filled *d* shell, from the presence of many interacting configurations at equivalent low energies. When using Kohn-Sham DFT, the XC energy is of pivotal importance. Indeed, we experienced, as others, the great fluctuations in spin splitting, spin-state orderings and ligation energies with functionals, some functionals providing results in contradiction with experimental trends. This issue has been discussed by Harvey⁴⁴ and systematized by Radon⁴⁵. After comparison with results obtained by Hunt *et al.*⁵ on 6C $[\text{MI-Fe}^{\text{III}}(\text{TPP})\text{-NO}]^+$, the B3LYP with TZP and TZVP were chosen, in agreement with Radon⁴⁵ to estimate the relative spin-state stabilities in single point calculations. These latter calculations were carried out with the Gaussian09⁴⁶ program suite on the previously optimized geometries with OPTX-PBE functionals. We have employed two different basis sets of TZP and def2-TZVP for all atoms. The selection of functional/basis sets was based on a benchmark study which was performed on the relative energies of the different spin states of Fe^{III} -porphyrin systems and the binding energy of the porphyrin-NO complex⁴. The BSSE (Basis Set Superposition Error) has been calculated with the counterpoise method of Boys and Bernardi⁴⁷ and is reported in Table 5. BSSE varies between .9 and 3 kcal.mol⁻¹ at the B3LYP/TZP level of theory and 0.2 and 1 kcal.mol⁻¹ at the B3LYP/def2-TZVP level.

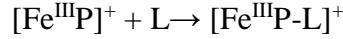
4. Results

4. 1. Experimental results

The affinity of small ligands was determined by temperature dependent equilibrium measurements between ligated and unligated ferric heme ions with a small ligand, in 5C and in 6C. The variation of the equilibrium between $[\text{Fe}^{\text{III}}\text{P}]^+$ and its $[\text{Fe}^{\text{III}}\text{P-L}]^+$ complex with temperature allows a determination of the bonding enthalpy of a ligand L with heme via the van't Hoff equation:

$$\frac{d(\ln K_p)}{dT} = \frac{\Delta_r H}{RT^2}$$

The enthalpy change ($\Delta_r H$) of the complexation reaction:



is obtained by multiplying the slope of a plot of $\ln K_p$ versus $1/T$ by R , where K_p is the constant pressure equilibrium constant, T the absolute temperature in Kelvin and R the ideal gas constant. This method has two advantages: i) it does not require the knowledge of *absolute number densities* of the reagents and is independent of entropy measurements, ii) experimentally the temperature is controlled within 2 K, while the setup allows sufficient collisions with the background helium gas to reach thermal equilibrium (see ref ¹²). $K_p(T)$ is determined by the measurements of the ratio of the intensity of the complex to that of the free heme ion: $I_{[\text{Fe}^{\text{III}}\text{P-L}]^+} / I_{[\text{Fe}^{\text{III}}\text{P}]^+} = K_p(T) \cdot p_L$, for each temperature. $I_{[\text{Fe}^{\text{III}}\text{P-L}]^+}$ and $I_{[\text{Fe}^{\text{III}}\text{P}]^+}$ represent the area of the corresponding mass peaks in Figure 2, p_L is the partial pressure of the ligand. The validity of measurements is provided by a linear van't Hoff plot, as in Figure 4, over the temperature variation interval.

In Figure 4, van't Hoff plots are represented for the ligation of CO (a) and O₂ (b) to $[\text{Fe}^{\text{III}}\text{P}]^+$ and $[\text{MI-Fe}^{\text{III}}\text{P}]^+$ at the same partial pressure. The resulting $\ln([\text{Fe}^{\text{III}}\text{P-CO}]^+ / [\text{Fe}^{\text{III}}\text{P}]^+)$ and $\ln([\text{MI-Fe}^{\text{III}}\text{P-CO}]^+ / [\text{MI-Fe}^{\text{III}}\text{P}]^+)$ plots with $1/T$ are linear in different temperature ranges. The equal concentration of ligated and free complex is indicated by a dotted line in Figure 4a. In Figure 4-a, it appears that the temperature of equal concentration in 6C, (T_1) of $[\text{MI-Fe}^{\text{III}}\text{P-CO}]^+$ and $[\text{MI-Fe}^{\text{III}}\text{P}]^+$ was accomplished at a much lower temperature, $T_1 = 47$ K than in 5C ($T_1=120$ K). Indeed, at 120 K (T_1 in 5C), the ratio of ligation of CO in 6C only amounts to $2.5 \cdot 10^{-3}$. The temperatures of equal concentration T_1 are thus a very sensitive means of scaling the relative affinities of ligands in 5C and 6C. Also, in the same pressure conditions, it is observed that ferric heme binds more strongly CO in 5C, as compared to O₂, accompanied by $T_1^{\text{CO}} > T_1^{\text{O}_2}$. Comparing 6C and 5C coordination of O₂ leads to the same results as for CO with a reduction of the binding energy by a factor of ≈ 3 , as reported in Table 1. This binding energy decrease by 6C coordination of O₂ is accompanied by a corresponding decrease of the T_1 temperature compared to that of 5C ferric heme O₂ results in Ref. ¹¹. Table 1 summarizes the experimental binding energies of different ligands (O₂, CO, NO) with 5C and 6C ferric heme and a comparison is made between the effects of two σ donors MI and histidine in $[\text{MP11 2H}]^{3+}$ in 5th axial coordination.

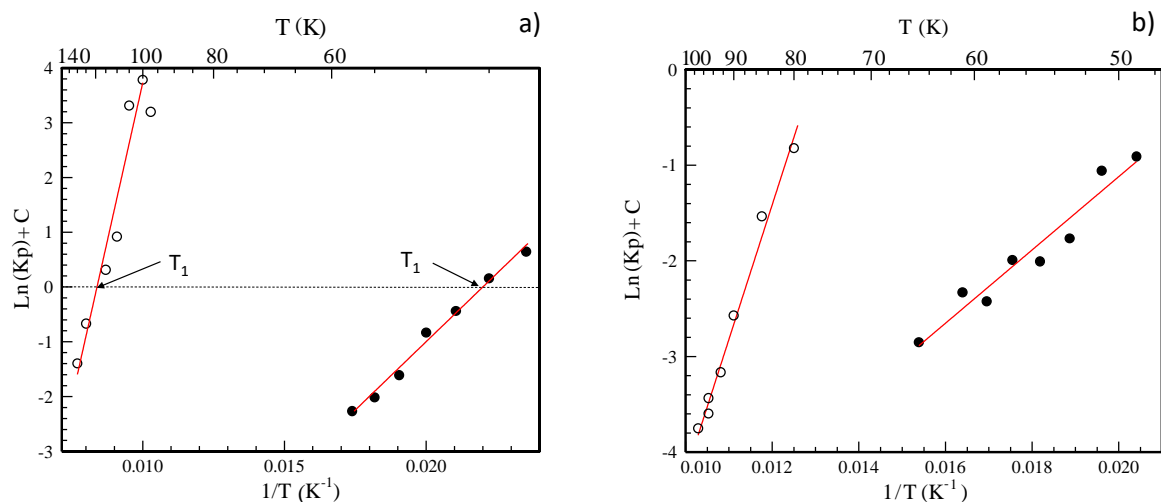


Figure 4: van't Hoff diagrams for the equilibrium between:

a) $[\text{Fe}^{\text{III}}\text{P-CO}]^+$ and $\text{CO}+[\text{Fe}^{\text{III}}\text{P}]^+$ (5C bond), empty circles; $[\text{MI-Fe}^{\text{III}}\text{P-CO}]^+$ and $\text{CO}+[\text{MI-Fe}^{\text{III}}\text{P}]^+$ (6C bond), filled circles. The dotted line corresponds to the equal concentrations of ligated and free $[\text{Fe}^{\text{III}}\text{P}]^+$

b) $[\text{Fe}^{\text{III}}\text{P-O}_2]^+$ and $\text{O}_2+[\text{Fe}^{\text{III}}\text{P}]^+$ (5C bond), empty circles; $[\text{MI-Fe}^{\text{III}}\text{P-O}_2]^+$ and $[\text{MI-Fe}^{\text{III}}\text{P}]^+$ (6C bond), filled circles.

Bottom axis: inverse temperatures, Kelvin^{-1} ; top axis Kelvin; left axis natural logarithm of the equilibrium constant + C, $(C = \text{Ln}(P_L))$; P_L is the ligand partial pressure (see text).

Complex	E_b (kcal mol $^{-1}$)
$[\text{Fe}^{\text{III}}\text{P-O}_2]^+$	-2.26 ± 0.26^{11}
$[\text{MI-Fe}^{\text{III}}\text{P-O}_2]^+$	-0.60 ± 0.14
$[\text{MP11 2H -O}_2]^{3+}$	-0.69 ± 0.14
$[\text{Fe}^{\text{III}}\text{P-CO}]^+$	-4.63 ± 0.43
$[\text{MI-Fe}^{\text{III}}\text{P-CO}]^+$	-0.86 ± 0.18
$[\text{MP11 2H -CO}]^{3+}$	-1.06 ± 0.18
$[\text{Fe}^{\text{III}}\text{P-NO}]^+$	$-24.88 \pm 0.71^{48,8}$
$[\text{MP11 2H-NO}]^{3+}$	-3.65 ± 0.17

Table 1: Experimental extrapolated binding energies ($E_b = \Delta_r H - 3/2 k_b T_1$) of O_2 , CO and NO with $[\text{Fe}^{\text{III}}\text{P}]^+$ in fifth or sixth axial coordination.

We also verified that the σ donor effect was not specific to N-methyl imidazole and repeated the experiment by measuring the ligation of the doubly protonated microperoxydase,

[MP11 2H]³⁺ (schemed in Figure 2, bottom) with O₂, CO and NO in 6C. The binding energy derived from the van't Hoff measurements and temperature corrections indicates a similar effect in the ratio of binding energies: $E = -0.69 \pm 0.14 \text{ kcal.mol}^{-1}$ ($-241 \pm 50 \text{ cm}^{-1}$, [MP11 2H-O₂]³⁺) as compared to the 5C heme value $E = -2.26 \pm 0.26 \text{ kcal.mol}^{-1}$ ($-790 \pm 90 \text{ cm}^{-1}$, [Fe^{III}P-O₂]⁺) (See Table 1). NO was coordinated to [MP11 2H]³⁺ and a small value for the ligation energy was found $3.63 \pm 0.17 \text{ kcal.mol}^{-1}$ ($1275 \pm 60 \text{ cm}^{-1}$), which represents a smaller value by a factor of ≈ 7 with respect to the 5C species observed in an ICR trap at room temperature^{8, 48}.

4-1-3 Photodissociation spectra of heme-imidazole complexes

When [MI-Fe^{III}-P-O₂]⁺ is photoexcited it can dissociate in several fragments: [MI-Fe^{III}-P]⁺ and [Fe^{III}-P]⁺ with the loss of simply O₂ or that of O₂ and MI. The ligation of methylimidazole (MI) with ferric heme was investigated by detecting the loss of MI and O₂, after exciting [MI-Fe^{III}-P-O₂]⁺. One obtains the spectrum in red in Figure 5 that shows a cut-off at 560 nm, as indicated by the dashed line. This spectrum can be compared with that obtained by monitoring only the loss of O₂ on the same complex in the same experiment. In Figure 5, the O₂ loss spectrum, blue trace, is strikingly different, extending to 650 nm. O₂ is a very weakly bound tag attached by $0.69 \text{ kcal.mol}^{-1}$ to [MI-Fe^{III}-P]⁺ (Table 1 *Table I*). Therefore the latter O₂ loss action spectrum is comparable to an absorption spectrum of the [MI-Fe^{III}-P]⁺ complex⁴⁹, with unit efficiency for the O₂ detachment. In contrast, the red spectrum is related to the dynamics of the loss of MI in the [MI-Fe^{III}-P]⁺ complex after evaporation of the O₂ tag.

A similar system to [MI-Fe^{III}P]⁺ has been investigated by Wyer et al.⁵⁰, the [Histidine-Fe^{III}P]⁺ pentacoordinated complex, obtaining its absorption spectrum in the gas phase at room temperature. Histidine is the natural σ donor to heme that is mimicked by MI. The [Histidine-Fe^{III}P]⁺ absorption spectrum is represented in Figure 5 by a black dashed line. It has a similar extension and bands as the O₂ detachment action spectrum, (blue).

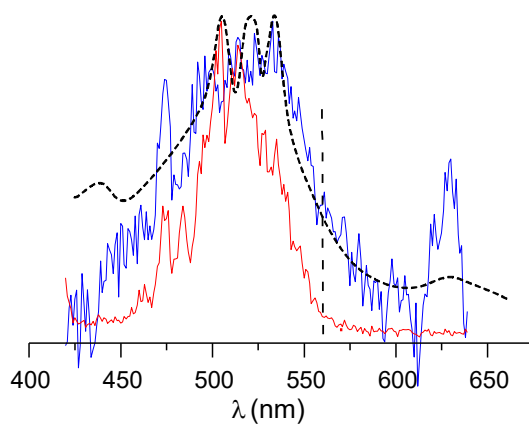


Figure 5: Photodissociation spectra of MI complexes. Red: Excitation of $[MI-Fe^{III}P-O_2]^+$ with MI and O_2 loss and detection of $[Fe^{III}P]^+$. Blue: excitation of $[MI-Fe^{III}P-O_2]^+$, O_2 loss and detection of $[MI-Fe^{III}P]^+$. The vertical axis for the blue and red curves represents the relative fragment yield, the ratio of fragment ions over the initial ion populations. Dotted line in black: absorption spectrum of $[Histidine-Fe^{III}P]^+$ in the gas phase from ref⁵⁰.

4. 2. Theoretical Results

The 5C and 6C complexes have been structurally characterized and their binding energies evaluated.

4. 2. 1. Structural Parameters

The geometries of $[Fe^{III}P]^+$ with O_2 , CO and NO with and without methylimidazole were optimized. The optimized geometry parameters are presented in Table 2. More details of the Cartesian coordinates can be found in the ESI file. The results show that the optimized structures of the $[Fe^{III}P]^+$ species in the doublet and quartet spin states are planar, while a strong out-of-plane deformation of the ferric centre associated with a domed structure is found for sextet states. On the other hand, ligation of MI results in a negative out-of-plane movement of the Fe atom towards MI, in all spin states of $[MI-Fe^{III}P]^+$. It is worth mentioning that the porphyrin ring in the doublet state is slightly distorted by ruffling. Also, inspection of Table S1 in ESI shows that ligation to $[Fe^{III}P]^+$, significantly affects other geometry parameters in all spin states.

The strongest bond among the small ligands studied relates to the low-spin state of the NO complex, as characterized by a very short bond length of 1.60 \AA . On the other hand, 5C NO binding to the porphyrin, causes a Fe doming in the low spin state, compared to the bare

porphyrin. The Fe–N–O angle is 180° in 5C and 6C, while a bent structure has been predicted in triplet and quintet states (see Fe–X–O angles, Table S1 in ESI) .

	S	Fe–XO	X–O	Doming ^a	∠FeXO	Fe–N _P ^b
Free [Fe^{III}P]⁺						
[Fe ^{III} P] ⁺	3/2	-	-	0.000	-	1.96
5 Coordinated [Fe^{III}P–L]⁺ (L=XO)						
[Fe ^{III} P–O ₂] ⁺	5/2	3.61	1.22	–0.05	108.6	1.96
[Fe ^{III} P–CO] ⁺	3/2	2.32	1.14	0.17	179.9	1.97
[Fe ^{III} P–NO] ⁺	0	1.60	1.16	0.33	180.0	1.99
<i>Exp. Values</i> ⁵¹	0	1.64	1.15	-	178.3	1.99
[MI–Fe^{III}P]⁺						
[MI–Fe ^{III} P] ⁺	5/2	-	-	–0.43	-	2.07
<i>Exp Values</i> ¹⁴				–0.360		2.038
6 Coordinated [MI–Fe^{III}P–L]⁺						
[MI–Fe ^{III} P–O ₂] ⁺	5/2	3.53	1.22	–0.18	88.21	1.98
[MI–Fe ^{III} P–CO] ⁺	5/2	3.49	1.15	–0.32	179.3	2.06
[MI–Fe ^{III} P–NO] ⁺	0	1.62	1.15	0.06	179.3	2.00
<i>Exp. Values</i> ⁵¹	0	1.63	1.15	-	176.3	2.00

Table 2: Selected optimized geometry parameters (in Å and degree, respectively for bond lengths and bond angles), for selected spin states. A description of the coordinates is reported in Figure 3. N_p indicates the pyrrolic nitrogens, L Labels the Ligand (O₂, CO and NO) a) The displacement of the Fe from the porphyrin plane is defined as doming. b) Average value of the four Fe–N_p bond lengths

There are rare X-ray crystallography structures for ferric heme systems^{14, 51}. Scheidt et al.¹⁴ extensively studied the [MI–Fe^{III}–OEP]⁺ (OEP stands for octa-ethylporphyrin) structure via X-ray crystallography and Mössbauer spectroscopy. They reported 2.038 Å and 0.360 Å for the Fe–N_p distance and the out-of-plane distortion of Fe from porphyrin plane, respectively. As

shown in Table 2 and Table S1 of ESI, our theoretical values of 2.07 and 0.43 Å are comparable with the corresponding results of Scheidt et al¹⁴. Recently, McQuarters⁵¹ and co-workers structurally characterized the 5C and 6C complexes of [Fe^{III}TPP]⁺ systems accompanied with different counter-ion moieties (TPP stands for tetra-phenyl porphyrin). They reported the Fe-Np and Fe-NO bond lengths being within the 1.994-1.996 Å and 1.640-1.665 Å range respectively for different counter-ions to [Fe^{III}TPP-NO]⁺. They also reported the corresponding values of 2.001 and 1.627 Å for the 6C [MI-Fe^{III}TPP-NO]⁺ systems. Inspection of Table 2 confirms that our theoretical distances are in agreement with the corresponding experimental values of McQuarters et al⁵¹. The experimental Fe∠NO angle⁵¹ in Table 2 is also found close to the 180° calculated value.

Upon coordination of MI, Fe–X distances in CO and NO complexes in all spin states (except for the quartet state of the CO complex) are increased with respect to the corresponding values in 5C complexes (Table S1). Overall, the ligation of MI diminishes the affinity of the ferric heme group for binding of the small ligands. It also obviously affects the electronic structure in all spin states, which is reflected on the change of the distortion of the porphyrin ring (see Figure S1, ESI file) and other structural parameters collected in Table S1.

4. 2. 2. The stability of spin states

In Table 3, we present the lowest energy spin states of the complexes of each ligand with [Fe^{III}P]⁺ or [MI-Fe^{III}P]⁺ systems derived from experiment, calculations or both. Considering the difficulties of the calculations, whenever possible, we consider the values determined experimentally. The concordance obtained in the experimental - theoretical structures and the agreement in the determination of the lowest energy spin state of several systems are considered as sensitive tools for qualifying functionals and basis sets.

Complex	S	Determination
$[\text{Fe}^{\text{III}}\text{P}]^+$	3/2	Exp. ¹³ and Calc.*
$[\text{MI-Fe}^{\text{III}}\text{P}]^+$	5/2	Exp. ¹⁴
	3/2	Calc.*
$[\text{Fe}^{\text{III}}\text{P-CO}]^+$	3/2	Exp. ⁶ and Calc.*
$[\text{MI-Fe}^{\text{III}}\text{P-CO}]^+$	5/2	Calc.*
$[\text{Fe}^{\text{III}}\text{P-O}_2]^+$	5/2	Calc.*
$[\text{Fe}^{\text{III}}\text{P-NO}]^+$	0	Exp. ⁵ and Calc.*
$[\text{MI-Fe}^{\text{III}}\text{P-NO}]^+$	0	Exp. ⁵ and Calc. ⁴

Table 3: Lowest energy spin states of ferric-porphyrin complexes. Exp. for experiment and Calc. for B3LYP/TZP calculations. *This work.

All spin states were calculated at the B3LYP level with the TZP basis sets. Calculations have been carried out with several ligands of decreasing strengths: NO and CO and O₂. The relative separation between spin states is found in Table S2 (ESI).

The ground spin state for $[\text{Fe}^{\text{III}}\text{P}]^+$ is the intermediate spin, quartet ($S=3/2$), in accordance with experimental evidence by Fang *et al.*¹³. For $[\text{MI-Fe}^{\text{III}}\text{P}]^+$, the quartet state is calculated 5.5 kcal.mol⁻¹ below the experimentally found sextet spin state¹⁴. We shall, as mentioned above, take the sextet state as the reference ground state in $[\text{MI-Fe}^{\text{III}}\text{P}]^+$ and derive bindings from this state.

Interestingly, one sees in Table 3 that the binding of NO in 5C and 6C hemes is accompanied with a spin state switching to the low spin state $S=0$, from $[\text{Fe}^{\text{III}}\text{P}]^+(S=3/2) + \text{NO}(S=1/2)$ and $[\text{MI-Fe}^{\text{III}}\text{P}]^+(S=5/2) + \text{NO}(S=1/2)$ respectively. These predicted stable states are in agreement with the previous theoretical⁴³ and experimental^{15, 51, 52} results.

In contrast, for CO, the 5C complex is found in the intermediate spin, $S=3/2$ correlating with the ground state of $[\text{Fe}^{\text{III}}\text{P}]^+ S=3/2$, in agreement with IR-PD spectroscopic results of Dillinger

*et al.*⁶ For the 6C complex, a high spin state 5/2 is lowest in energy and we consider the binding to the reference state $[\text{MI-Fe}^{\text{III}}\text{P}]^+ S=5/2$.

O_2 ligates also $[\text{Fe}^{\text{III}}\text{P}]^+(S=3/2)$, without spin crossover in $S=5/2$, owing to the spin $S=1$ of O_2 . This configuration is confirmed by examining the electron distribution via the spin density. Representing the spin density for the different complexes, isosurfaces are displayed in Table 4. For $[\text{Fe}^{\text{III}}\text{P}]^+ (S=3/2)$, the spin density corresponding to the 3 unpaired electrons is mainly concentrated on the Fe atom with an integrated spin density of 2.877 on iron (according to the Mulliken scheme) equivalent to three unpaired electrons. The same holds for $[\text{Fe}^{\text{III}}\text{P-CO}]^+ (S=3/2)$. The $[\text{Fe}^{\text{III}}\text{P-O}_2]^+ (5/2)$ complex, has a similar (2.785) spin density on the Fe atom indicating that the complex has similar electronic properties as $[\text{Fe}^{\text{III}}\text{P-CO}]^+$, but with ($S=1$) for O_2 (see ESI Table S3).

In turn, the high spin imidazole complexes $[\text{MI-Fe}^{\text{III}}\text{P}]^+$ and $[\text{MI-Fe}^{\text{III}}\text{P-CO}]^+$ show a high spin density on the Fe atom (4.208), but share some of their high spin density ~ 0.4 , with the neighbouring pyrrolic nitrogen Np atoms.

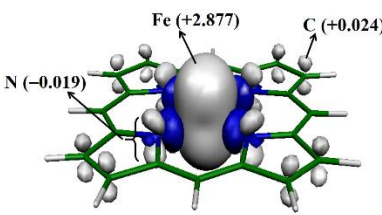
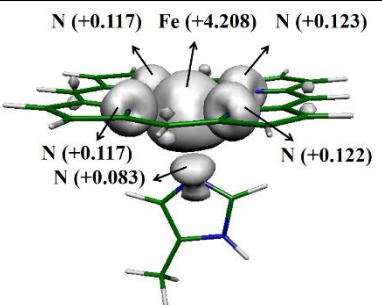
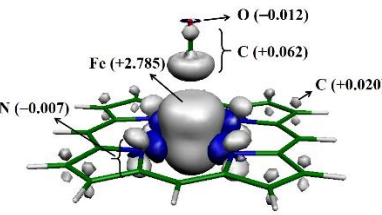
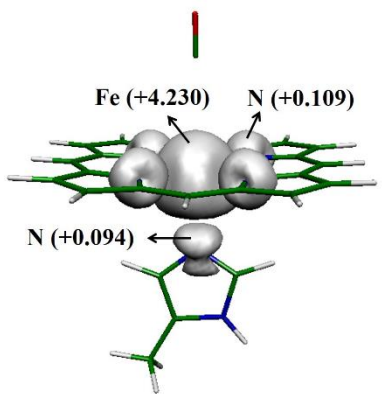
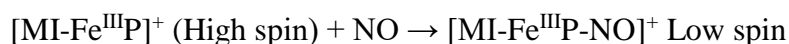
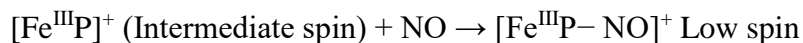
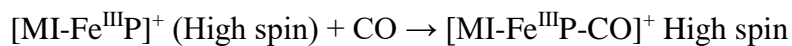
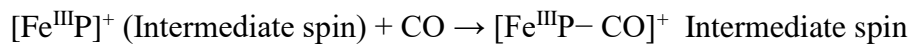
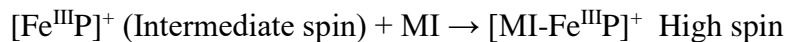
Complex	Spin	Spin Density Plot (isosurface=0.0025)	Complex	Spin	Spin Density Plot (isosurface=0.0025)
$[\text{Fe}^{\text{III}}\text{P}]^+$	3/2		$[\text{MI-Fe}^{\text{III}}\text{P}]^+$	5/2	
$[\text{Fe}^{\text{III}}\text{P-CO}]^+$	3/2		$[\text{MI-Fe}^{\text{III}}\text{P-CO}]^+$	5/2	

Table 4: Computed spin density of $[\text{Fe}^{\text{III}}\text{P}]^+$, $[\text{MI-Fe}^{\text{III}}\text{P}]^+$ and $[\text{MI-Fe}^{\text{III}}\text{P-L}]^+$: spin-up and spin-down densities are shown as white grey and blue, respectively.

4.2.3 Ligand binding energies

It is reasonable to postulate that weak ligands CO, O₂ and N₂¹¹ cannot change the spin state of the strongly coordinated [MI-Fe^{III}P]⁺

According to Table 3, the following equations are satisfied during ligation:



CO binds rather efficiently ferric heme without spin change in 5C, while NO binds more strongly with spin crossing. On the other hand, the calculated ferric bond energy with O₂ is small close to 0, within the precision of the calculations.

Complex	Spin State	B3LYP/TZP		B3LYP/def2-TZVP		Experiment
		E _b (kcal mol ⁻¹)	BSSE	E _b (kcal mol ⁻¹)	BSSE	E _b (kcal mol ⁻¹)
[MI-Fe ^{III} P] ⁺	5/2	-27.80	2.40	-26.28	1.11	< -51
[Fe ^{III} P-CO] ⁺	3/2	-8.42	2.27	-6.57	0.63	-4.63±043
[MI-Fe ^{III} P-CO] ⁺	5/2	-0.73	0.88	-0.05	0.26	-0.86±014
[Fe ^{III} P-NO] ⁺	0	-9.32	3.10	-34.4 ⁸		-24.88±0.71 ⁴⁸
[MP11 2H-NO] ³⁺	0	*		-3.9 ^a		-3.65±0.17

Table 5: Binding energies of penta- and hexa-coordinated ferric [Fe^{III}P]⁺. Notes. a) The theoretical value for the binding energy of NO to [MI-Fe^{III}P]⁺ system is the same as in ref⁴, determined at the B3LYP/TZVP level of theory.

MI forms a strong bond with [Fe^{III}P]⁺ with 26 kcal.mol⁻¹ and its σ donating lone pair promotes the high spin state for the complex, as observed by Scheidt *et al.*¹⁴ Therefore ligation of [MI-

$\text{Fe}^{\text{III}} \text{P}]^+ (5/2)$ will result in a high spin 6C complex, unless a deeper potential from a different spin state would cross, like for the NO complex ^{4, 5}.

As shown in Table 5, ligation of CO in 6C $[\text{MI-Fe}^{\text{III}}\text{P-CO}]^+ (S=5/2)$ results in a strong decrease in the binding energy as compared to the 5C $[\text{Fe}^{\text{III}}\text{P-CO}]^+$ and taking account the BSSE the binding energy is close to 0 kcal.mol⁻¹.

It is noteworthy that the obtained energetic results in this section confirm those derived from structural parameters in previous section, associating short Fe-ligand bonds with higher bond energies.

5-Discussion

Measuring binding energies is a direct way to characterize the bond properties of heme complexes. Ferrous porphyrins experience high ligation energies and this has been shown to arise from spin crossover between free and ligated porphyrins. The spin crossover between the initial $\text{Fe}^{\text{II}} (S=2)$ and final $\text{Fe}^{\text{II}} (S=0)$ typifies a reorganization of the Fe atom electrons in their lowest lying 3d orbitals. There, the crossover allows for a stronger interaction with the σ donation from the incoming ligand and the now free Fe ($3d_{z^2}$) orbital. This combines with a Fe ($3d_{xz,yz}$) π interaction with the ligand π^* free orbitals, the so-called π backdonation. The ligation of O_2 to Fe^{II} porphyrins results from the passage of the high spin heme-ligand adducts into a deep potential descending from a higher energy $S=0$ spin state ⁵³.

In the case of ferrous $\text{Fe}^{\text{II}}\text{-O}_2$ ligation, the scheme is triggered by an initial electron transfer from Fe to O_2 . This electron transfer from the Fe atom cannot happen for ferric hemes, already bearing a positive charge on Fe. Ferric hemes experience in general lower binding energies and the above mechanism of spin crossing is not effective, except for the NO ligand. Nonetheless, binding in ferric hemes is linked to ligand σ donation and π retrodonation.

Few ligands (NO and H_2O) bind ferric heme at room temperature and we discuss here the fact that this binding is decreased for hexacoordinated ferric porphyrins with MI compared to pentacoordination. MI coordinates by forming a σ combination of its imidazole nitrogen lone pair sp^2 orbital with $\text{Fe}(3d_{z^2})$; this, of course, strongly interferes with the equivalent pairing with small ligands in 6th coordination.

5-1 Binding energies

In pentacoordinated heme, the binding energies in ferric complexes follow a well defined trend: $E(\text{NO})^{48} > E(\text{CO}) > E(\text{O}_2)^{11} > E(\text{N}_2)^{11}$. Indeed, as noted in Table 1 and Table 5, NO binds ferric porphyrins with $24.9 \pm 0.7 \text{ kcal.mol}^{-1}$ ($8710 \pm 240 \text{ cm}^{-1}$)⁴⁸, while N_2 binds with $0.54 \pm 1 \text{ kcal.mol}^{-1}$ ($189 \pm 35 \text{ cm}^{-1}$)¹¹. The order of the binding energy of $[\text{Fe}^{\text{III}}\text{P-L}]$ is in agreement with the order of the observed equal concentration temperatures T_1 , $T_1(\text{NO}) > T_1(\text{CO}) > T_1(\text{O}_2) > T_1(\text{N}_2)$, of the complexes in the ion trap. Except for $[\text{Fe}^{\text{III}}\text{P-NO}]^+$ and strong σ donors, the formation of 5C complexes does not lead to spin crossover. As mentioned earlier, the binding mechanism involves an initial σ donation to the half-filled Fe ($3d_{z^2}$), thus less efficient than for an empty Fe ($3d_{z^2}$) orbital¹¹. Therefore, the strength of the bond with ferric heme ($S=3/2$) is conditioned by the back donation from Fe ($3d_{xz,yz}$) that ensures the relative efficiency of the different ligands, where CO is an efficient acceptor as compared with O_2 . Indeed, CO donates via C($p\sigma$) to Fe($3d_{z^2}$), while it accepts in its free π^* orbitals electrons from Fe($3d_{xz,yz}$). Calculations (Table 2) show a linear Fe-CO geometry indicative of this backdonation in the two CO π^* orbitals more localised on the C atom. Calculations of the energy of the Fe-CO geometry as compared to that of Fe-OC (ten times weaker) confirms $[\text{FeP}^{\text{III}}\text{-CO}]^+$ as the stable complex, as reported in table S4 in ESI.

The ferric heme O_2 complex has a similar electronic configuration for the Fe^{III} cation, as shown in the Mulliken spin analysis (vide supra). It is however more weakly bound than CO and adopts a bent Fe- O_2 geometry $\angle\text{FeXO}=108.6^\circ$ (Table 2) since only one O_2 π^* orbital is available for backdonation. N_2 with its triple bond has not much room for backdonation and we observe only a very weakly bound 5C complex¹¹. A correlation between the efficiency of backdonation and the binding energies can be invoked in 5C ferric heme complexes. Note that the binding energies $< 5 \text{ kcal.mol}^{-1}$ are inferior to the calculated spin state splittings (see Table S2 in ESI).

The situation is distinct for $[\text{Fe}^{\text{III}}\text{P-NO}]^+$, where it is established that the ferric heme NO complex has total spin $S=0$ ⁵¹; therefore a spin crossover is required from the initial $[\text{Fe}^{\text{III}}\text{P}]^+$ ($3/2$)+ NO($1/2$) pair. Praneeth⁴ discussed in details the crossover in the case of the 6C complex with two successive potential crossings from the initial $[\text{MI-Fe}^{\text{III}}\text{P}]^+$ ($5/2$)+ NO($1/2$) complex. This leads to a rather deep potential, which ultimately crosses a $[\text{Fe}^{\text{II}}\text{P-N}^+\text{O}]$ ($S=0$) potential at 1.69\AA close to the bottom of the well at 1.6\AA . The $[\text{MI-Fe}^{\text{II}}\text{P-N}^+\text{O}]$ singlet complex can

experience strong backbonding from Fe ($3d_{xz, yz}$) to the two free π^* NO orbitals⁵¹. In contrast, $[\text{MI-Fe}^{\text{III}}\text{P-CO}]^+$ and $[\text{MI-Fe}^{\text{III}}\text{P-O}_2]^+$, do not involve spin crossing.

5-2 MI binding energy

We linked in the results, section 4-I-3, the O₂ loss spectrum (blue line, Figure 5) of $[\text{MIFe}^{\text{III}}\text{P-O}_2]^+$ to the absorption spectrum of $[\text{MI-Fe}^{\text{III}}\text{P}]^+$ since O₂ is only a weakly bound tag as previously mentioned⁴⁹. On the other hand, in comparing the blue and red curves in Figure 5, when the loss of strongly bound MI is detected, a threshold is apparently reached at 560 nm to allow the dissociation of MI.

The calculated value for the dissociation is 26.3 kcal.mol⁻¹ for the MI bond energy in $[\text{MI-Fe}^{\text{III}}\text{P}]^+$. This dissociation cannot occur within an excited electronic state with insufficient excess energy for direct dissociation. Thus dissociation will proceed from a vibrationally hot $[\text{MI-Fe}^{\text{III}}\text{P}]^+$ ground state, through a statistical process, after evaporation of O₂. The energy threshold at 51 kcal.mol⁻¹ (at 560 nm) is higher than the 27 kcal.mol⁻¹ calculated total binding energy (Table 5) and from the Arrhenius barrier to dissociation found at 1.4 ± 0.2 eV (32 ± 6 kcal.mol⁻¹)⁹ for the similar system, $[\text{Histidine-FeP}]^+$ and obtained at room temperature with a substantial internal energy. The higher threshold observed at 51 kcal.mol⁻¹ could correspond to the necessary energy excess for an adapted dissociation time to our experimental time window (40 ms) and our temperature ~ 40 K, with low internal energy. Therefore, 51 kcal.mol⁻¹ is certainly a higher limit for the dissociation energy of the Fe-MI bond.

Such a strong binding, between MI and $[\text{FeP}]^+ > \sim 26$ kcal.mol⁻¹ ensures the stability of heme to photoexcitation in the globin pocket of hemoproteins, where ferric heme in the biological context, will quickly relax its excess energy to the surrounding medium, thus preserving this bond.

5-3 Hexacoordinated ferric heme

The effect of MI ligated in 5th position is dramatic, as seen in Figure 4, where the ligation energy of O₂ and CO drops by a factor between 4 and 5. Energy calculations confirm this trend, unambiguously for 5C/6C ferric CO complexes as shown in Table 5, where the 5C complex is bound by 6.57 kcal.mol⁻¹ (B3LYP/def2-TZVP), compared to 0.05 kcal.mol⁻¹ for the 6C complex. In addition, when taking the BSSE into account, the 6C complex is unbound at this

level of theory. The destabilization effect promoted by MI is equally apparent in the Fe-CO lengthening from 2.32 to 3.49 Å (Table 2).

Concerning the 6C NO complex, the effect of MI *trans* axial ligand bonding is also striking, where the experimental binding energy is reduced from 24 to 3.65 kcal.mol⁻¹. The *trans* axial ligand effect has been investigated in details by Praneeth *et al.*⁵⁴ in the case of Fe^{II} porphyrins with the NO ligand. From equilibrium constants, it was found that the binding strength of NO to Fe^{II} ligand is considerably reduced in 6C with a strong σ donor like MI in *trans* axial position. This shows also in the smaller NO force constant in 6C with respect to 5C. The central mechanism for bonding in Fe^{II}-NO is the σ bonding of NO (π^*) to Fe ($3d_{z^2}$). As described by Praneeth *et al.*⁵⁴, the covalency of this bond can be continuously changed, ranging from Fe^{III}NO⁻ to Fe^INO⁺, depending upon the character of the σ donor in 6C. The decrease in the NO force constant in 6C is assigned to a greater presence of the antibonding π^* electron on NO, weakening this bond and showing a decrease of σ donation to Fe ($3d_{z^2}$). The Fe-NO bond strength is highly influenced by the competition for Fe($3d_{z^2}$) between MI (nitrogen sp^2 pair) and NO(π^*), in sixth coordination⁵.

This competition for Fe($3d_{z^2}$) occupancy can be transposed to the ligation of Fe^{III} with CO, where the Fe-L distance lengthening upon 6th coordination can be analyzed as resulting from the competition between the strong σ donor MI and the smaller σ donor CO for Fe($3d_{z^2}$). This competition appears in the natural orbital occupancy of Fe($3d_{z^2}$) where the β spin occupancy in Fe($3d_{z^2}$) of [Fe^{III}P-CO]⁺ is 0.198, while that of the 6C [MI-Fe^{III}P-CO]⁺ increases to 0.218. Therefore, we surmise that another effect comes into play, the π backbonding discussed above and that ensures the strength of the bond in ferric heme. In 6C [MI-Fe^{III}P-CO]⁺, the Fe-CO σ bonding strength decrease, if accompanied by a notable Fe-CO bond lengthening, must affect the retro π bond to $\pi^*(CO)$ and weaken the Fe-CO bond. This stems from a sharp decrease in the π orbital overlap with interatomic distance. Indeed Fe-C=2.32 Å in [Fe P-CO]⁺, while it increases to 3.49 Å in [MI-Fe^{III}P-CO]⁺, as reported in Table 2. This comparison between penta and hexacoordinated ferric hemes is facilitated by the absence of spin crossing in the ligation process of CO and O₂. The discussion emphasizes that a combination of experimental and theoretical description of these complex systems allows reaching a more detailed picture of the factors influencing the ligand bond energy in 5C and 6C ferric heme complexes.

6-Conclusions

The sixth ligation to ferric heme has been investigated in presence of a σ donor in 5th axial ligation. The binding energy of ligands L=O₂, CO and NO with 5C Fe^{III}P and 6C MI-Fe^{III}P systems have been determined by the van't Hoff equation by maintaining a series of different temperatures in a Paul ion trap containing He-ligand mixtures. There, the equilibrium between unligated and ligated species is observed in a range comprising no complexation to complete complexation with a linear dependence of $\text{Ln}([\text{Fe}^{\text{III}}\text{P}^+-\text{L}]/[\text{Fe}^{\text{III}}\text{P}^+])$ with $(1/T)$. The cold ion trap setup allows the preparation and the characterization of ligation to hemes either in fifth or sixth position in a more controllable way than in solution allowing direct comparison with theoretical calculations.

Ferric heme binds weakly small ligands in 5C, and the result of these investigations is the dramatic effect of a σ donor in 5th position of ferric heme in decreasing the ligation energy of small ligands when in 6th position. The reduction for O₂, CO, NO is far less than minor since the fifth coordination of a σ donor (MI) leads to a decrease in the ligand binding energy in a ratio >3. This effect has been perfectly supported by DFT (B3LYP/ *def2*-TZVP) calculations in the case of [MI-Fe^{III}P-CO]⁺.

It is interesting to compare this above *trans* axial effect, as named by Lehnert *et al.*,^{4, 54} of a dramatic bond weakening in the case of ferric heme, with the same effect already observed for ferrous heme through Fe-ligand distance lengthening upon 6C⁵⁵. Ligands such as CO or O₂ that do not involve spin crossing in either 5C or 6C ferric hemes eases the comparison between calculations and observations. Fe (3d_{z²}) orbitals play a central role in the ligation of ferric as well as for ferrous hemes. Future experiments and calculations should endeavor to rationalize the influence of the interaction between pyrrolic Np orbitals and Fe (3d_{x²-y²}) orbitals, which are in strong interaction; the former Np orbitals serving as an electron reservoir for the Fe ligand interaction¹⁶.

7-Acknowledgments

This work was supported by the Center for International Scientific Studies and Collaboration (CISSC), French Embassy in Iran and the PHC Gundishapur 2016-2017 project n°35629XE. The research council of University of Isfahan is also acknowledged. We are grateful to Laboratoire de Chimie Physique of CNRS and the University of Paris-Sud for supporting our computations. M.E.C. is grateful to the University Paris-Sud for the “*Professeur invité*” position in 2016. The authors are thankful to Professor Simonetta Formarini for her active interest in this study. We thank GENCI for a generous time allocation on the CINES supercomputers (project number A0040806830).

References:

1. G. P. Roberts, R. L. Kerby, H. Youn and M. Conrad, *J. Inorg. Biochem.*, 2005, 99, 280.
2. B.-K. Yoo, I. Lamarre, J.-L. Martin, F. Rappaport and M. Negrier, *Proc. Natl. Acad. Sci. U.S.A.*, 2015, 112, E1697.
3. R. Makino, S.-y. Park, E. Obayashi, T. Iizuka, H. Hori and Y. Shiro, *J. Biol. Chem.*, 2011, 286, 15678.
4. V. K. K. Praneeth, F. Paulat, T. C. Berto, S. D. George, C. Näther, C. D. Sulok and N. Lehnert, *J. Am. Chem. Soc.*, 2008, 130, 15288.
5. A. P. Hunt and N. Lehnert, *Acc. Chem. Res.*, 2015, 48, 2117.
6. S. Dillinger, J. Lang and G. Niedner-Schatteburg, *J. Phys. Chem. A.*, 2017, 121, 7191.
7. T. Karpuschkin, M. M. Kappes and O. Hampe, *Angew. Chem. Int. Ed.*, 2013, 52, 10374.
8. B. Chiavarino, M. E. Crestoni, S. Fornarini and C. Rovira, *Inorg. Chem.*, 2008, 47, 7792.
9. M. K. Lykkegaard, H. Zettergren, M.-B. S. Kirketerp, A. Ehlerding, J. A. Wyer, U. Kadhane and S. B. Nielsen, *J. Phys. Chem. A.*, 2009, 113, 1440.
10. T. Archipov, J. Kirkland, K. D. Vogiatzis, A. Steiner, G. Niedner-Schatteburg, P. Weis, K. Fink, O. Hampe and M. M. Kappes, *J. Phys. Chem. A*, 2018.
11. L. Ferrand, S. Soorkia, G. Grégoire, M. Broquier, B. Soep and N. Shafizadeh, *Phys. Chem. Chem. Phys.*, 2015, 17, 25693.
12. N. Shafizadeh, S. Soorkia, G. Gregoire, M. Broquier, M. E. Crestoni and B. Soep, *Chemistry-a European Journal*, 2017, 23, 13493.
13. M. Fang, S. R. Wilson and K. S. Suslick, *J. Am. Chem. Soc.*, 2008, 130, 1134.
14. W. R. Scheidt, D. K. Geiger, Y. J. Lee, C. A. Reed and G. Lang, *J. Am. Chem. Soc.*, 1985, 107, 5693.
15. J. A. Wyer, A. V. Jørgensen, B. Møller Pedersen and S. Brøndsted Nielsen, *Chem. Phys. Chem.*, 2013, 14, 4109.
16. M. E. Ali, B. Sanyal and P. M. Oppeneer, *J. Phys. Chem. B*, 2012, 116, 5849.
17. C.-K. Siu, Y. Guo, A. C. Hopkinson and K. M. Siu, *J. Phys. Chem. B.*, 2006, 110, 24207.
18. O. Charkin, N. Klimenko, D. Charkin, H.-C. Chang and S.-H. Lin, *J. Phys. Chem. A.*, 2007, 111, 9207.
19. O. Charkin, N. Klimenko, P. Nguyen, D. Charkin, A. Mebel, S. Lin, Y.-S. Wang, S.-C. Wei and H.-C. Chang, *Chem. Phys. Lett.*, 2005, 415, 362.
20. V. E. Berryman, R. J. Boyd and E. R. Johnson, *J. Chem. Theory. Comput.*, 2015, 11, 3022.
21. M.-S. Liao, M.-J. Huang and J. D. Watts, *J. Phys. Chem. A.*, 2010, 114, 9554.
22. C. Rovira, K. Kunc, J. Hutter, P. Ballone and M. Parrinello, *J. Phys. Chem. A*, 1997, 101, 8914.
23. G. Féraud, M. Broquier, C. Dedonder-Lardeux, G. Grégoire, S. Soorkia and C. Jouvet, *Phys. Chem. Chem. Phys.*, 2014, 16, 5250.
24. V. E. Walker, N. Castillo, C. F. Matta and R. J. Boyd, *J. Phys. Chem. A.*, 2010, 114, 10315.
25. J. M. Ugalde, B. Dunietz, A. Dreuw, M. Head-Gordon and R. J. Boyd, *J. Phys. Chem. A.*, 2004, 108, 4653.
26. M. Radon and K. Pierloot, *J. Phys. Chem. A.*, 2008, 112, 11824.
27. V. E. Berryman, M. G. Baker and R. J. Boyd, *J. Phys. Chem. A*, 2014, 118, 4565.

28. A. M. Koster, G. Geudtner, A. Alvarez-Ibarra, P. Calaminici, M. E. Casida, J. Carmona-Espindola, V. D. Dominguez, R. Flores-Moreno, G. U. Gamboa, A. Goursot, T. Heine, A. Ipatov, A. de la Lande, F. Janetzko, J. M. del Campo, D. Mejia-Rodriguez, J. U. Reveles, J. Vasquez-Perez, A. Vela, B. Zuniga-Gutierrez and D. R. Salahub, *The deMon Developers*, Cinvestav, México City, 2016.
29. A. M. Koster, G. Geudtner, P. Calaminici, M. E. Casida, R. Flores-Moreno, J. Carmona-Espindola, G. U. Gamboa, A. Goursot, F. Janetzko, J. U. Reveles, A. Vela and B. Zuniga-Gutierrez, *The deMon2k Users' Guide, Version 3.0*, Cinvestav, México City, 2011.
30. P. E. Siegbahn, M. R. Blomberg and S.-L. Chen, *J. Chem. Theory Comput.*, 2010, 6, 2040.
31. E. R. Johnson and A. D. Becke, *Can. J. Chem.*, 2009, 87, 1369.
32. C. Rovira, K. Kunc, J. Hutter, P. Ballone and M. Parrinello, *Int. J. Quantum Chem.*, 1998, 69, 31.
33. H. Nakashima, J. Y. Hasegawa and H. Nakatsuji, *J. Comput. Chem.*, 2006, 27, 426.
34. M.-S. Liao and S. Scheiner, *J. Chem. Phys.*, 2002, 116, 3635.
35. M.-S. Liao, M.-J. Huang and J. D. Watts, *J. Phys. Chem. B*, 2013, 117, 10103.
36. Y. Kitagawa, Y. Chen, N. Nakatani, A. Nakayama and J. Hasegawa, *Phys. Chem. Chem. Phys.*, 2016, 18, 18137.
37. A. R. Groenhof, M. Swart, A. W. Ehlers and K. Lammertsma, *J. Phys. Chem. A*, 2005, 109, 3411.
38. M. C. Durrant, *Dalton Trans.*, 2014, 43, 9754.
39. B. Chiavarino, M. E. Crestoni and S. Fornarini, *Croat. Chem. Acta*, 2014, 87, 307.
40. H. Chen, M. Ikeda-Saito and S. Shaik, *J. Am. Chem. Soc.*, 2008, 130, 14778.
41. A. C. Chamberlin, A. Ikezaki, M. Nakamura and A. Ghosh, *J. Phys. Chem. B*, 2011, 115, 3642.
42. L. M. Blomberg, M. R. Blomberg and P. E. Siegbahn, *J. Inorg. Biochem.*, 2005, 99, 949.
43. A. Abdurahman and T. Renger, *J. Phys. Chem. A*, 2009, 113, 9202.
44. J. N. Harvey, *Annual Reports Section "C" (Physical Chemistry)*, 2006, 102, 203.
45. M. Radoń, *J. Chem. Theory Comput.*, 2014, 10, 2306.
46. M. J. Frisch, G. W. Trucks, H. B. Schlegel, G. E. Scuseria, M. A. Robb, J. R. Cheeseman, G. Scalmani, V. Barone, G. A. Petersson, H. Nakatsuji, X. Li, M. Caricato, A. Marenich, J. Bloino, B. G. Janesko, R. Gomperts, B. Mennucci, H. P. Hratchian, J. V. Ortiz, A. F. Izmaylov, J. L. Sonnenberg, D. Williams-Young, F. Ding, F. Lipparini, F. Egidi, J. Goings, B. Peng, A. Petrone, T. Henderson, D. Ranasinghe, V. G. Zakrzewski, J. Gao, N. Rega, G. Zheng, W. Liang, M. Hada, M. Ehara, K. Toyota, R. Fukuda, J. Hasegawa, M. Ishida, T. Nakajima, Y. Honda, O. Kitao, H. Nakai, T. Vreven, K. Throssell, J. J. A. Montgomery, J. E. Peralta, F. Ogliaro, M. Bearpark, J. J. Heyd, E. Brothers, K. N. Kudin, V. N. Staroverov, T. Keith, R. Kobayashi, J. Normand, K. Raghavachari, A. Rendell, J. C. Burant, S. S. Iyengar, J. Tomasi, M. Cossi, J. M. Millam, M. Klene, C. Adamo, R. Cammi, J. W. Ochterski, R. L. M. , K. Morokuma, O. Farkas, J. B. Foresman and D. J. Fox, Gaussian 09, Gaussian, Inc., Wallingford CT, 2013.
47. S. F. Boys and F. Bernardi, *Molecular Physics*, 1970, 19, 553.
48. O. Chen, S. Groh, A. Liechty and D. P. Ridge, *J. Am. Chem. Soc.*, 1999, 121, 11910.
49. M. A. Duncan, *Int. Rev. Phys. Chem.*, 2003, 22, 407.
50. J. A. Wyer and S. B. Nielsen, *J. Chem. Phys.*, 2010, 133, 084306.
51. A. B. McQuarters, J. W. Kampf, E. E. Alp, M. Hu, J. Zhao and N. Lehnert, *Inorg. Chem.*, 2017, 56, 10513.

- 52. J. A. Wyer and S. Brøndsted Nielsen, *Angew. Chem. Int. Ed.*, 2012, 51, 10256.
- 53. J. N. Harvey, *J. Am. Chem. Soc.*, 2000, 122, 12401.
- 54. V. K. K. Praneeth, C. Näther, G. Peters and N. Lehnert, *Inorg. Chem.*, 2006, 45, 2795.
- 55. C. Cao, S. Dahal, M. Shang, A. M. Beatty, W. Hibbs, C. E. Schulz and W. R. Scheidt, *Inorg. Chem.*, 2003, 42, 5202.